sustainability

MDPI

Article

Hydrokinetic Power Resource Assessment in a Combined Estuarine and River Region

Gianmaria Giannini [1,2,*], Victor Ramos [1,2], Paulo Rosa-Santos [1,2], Tomás Calheiros-Cabral [1,2] and Francisco Taveira-Pinto [1,2]

[1] Hydraulics, Water Resources and Environment Division, Department of Civil Engineering, Faculty of Engineering, University of Porto (FEUP), 4200-465 Porto, Portugal; jvrc@fe.up.pt (V.R.); pjrsantos@fe.up.pt (P.R.-S.); tcabral@fe.up.pt (T.C.-C.); fpinto@fe.up.pt (F.T.-P.)

[2] Interdisciplinary Centre of Marine and Environmental Research (CIIMAR), 4450-208 Matosinhos, Portugal

* Correspondence: gianmaria@fe.up.pt

Abstract: The worldwide river and tidal hydrokinetic power potential is considerable. Harnessing such potential could allow the generation of a significant amount of sustainable electricity for local uses. To the present, most studies on hydrokinetic power have focused on large-scale commercial technology development, large tidal farms planning, and high-intensity resources assessment. Reduced attention was oriented towards investigating possibilities for small to medium-size hydrokinetic plants. However, given the characteristics of rivers and estuaries, in most cases, relevant hydrokinetic power exploitation possibilities exist regardless of the dimensions of the region considered. The planning of small to medium-size hydrokinetic plants for various aspects differs from larger developments. In the present work, a method for assessing the hydrokinetic resource is proposed and applied to the case study of the Douro waterway, which is characterized by moderate flow speeds and limited water depths. A high-resolution shallow-water numerical model is set up using ocean and river inflow boundary conditions. The flow velocities are estimated for the neap-spring period for different freshwater discharges. The spots presenting the highest annual hydrokinetic power average were identified, maximum flow speeds of about 1 m/s were found, and an annual mean power of 0.4 kW/m^2 was estimated, indicating that prospects for hydrokinetic energy harvesting exist.

Keywords: tidal power; high-resolution numerical model; sites selection method; in-stream energy; Douro River tidal resource

Citation: Giannini, G.; Ramos, V.; Rosa-Santos, P.; Calheiros-Cabral, T.; Taveira-Pinto, F. Hydrokinetic Power Resource Assessment in a Combined Estuarine and River Region. *Sustainability* **2022**, *14*, 2606. https://doi.org/10.3390/su14052606

Academic Editor: M. Sergio Campobasso

Received: 27 January 2022
Accepted: 18 February 2022
Published: 23 February 2022

1. Introduction

Estuaries, fiords, and other similar coastal areas often have a considerable hydrokinetic energy potential, which can be harnessed for feeding the increasing energy demand of coastal communities. At these locations, the flow of water can mainly be driven by the tide phenomenon and, therefore, the water velocity pattern is highly cyclical and predictable, making the hydrokinetic resource a valuable source of energy [1]. Previous work mainly focused on the assessment of tidal power resources in large domains or straits (for example [2,3]). In contrast, for various aspects, the analysis of the hydrokinetic energy potential in smaller waterways may be different. For instance, at these locations, we have significant freshwater discharges, limited water depths, and complex morphology. Given these characteristics, an ad-hoc methodology is required to include these in the analysis to accurately assess the annual hydrokinetic energy potential.

Despite the high cost of existing in-stream tidal power, as well as in the case of other marine renewable energy technologies, several governmental supporting mechanisms and new marine planning policies are progressively becoming available, which aid the development of marine renewable energy plants [4]. Therefore, from one side, first prospects for commercial plants development exist, on the other side, new approaches and technical assessments are required to realistically evaluate the viability of new potential hydrokinetic

plants case by case. In this context, a holistic methodology is needed for evaluating the energy resource, and for systematically considering the major constraints for selecting the most suitable spots within a study region.

A considerable number of known locations having low to high hydrokinetic power potential are in Europe. Medium to high potential locations for tidal power plants development are situated in the United Kingdom [5], France [3], at the Strait of Gibraltar [6], and the Strait of Messina [7,8]. Furthermore, it is expected that several more hotspots having lower and unknown potential exist throughout the continent. As illustrated in Figure 1—which is adapted and extended based on information from [9]—for lower and unknown hydrokinetic potential sites, limited information exists. Therefore, there is a need for accurate investigation of the hydrokinetic resource for discovering new power production opportunities at the mentioned places. As initially mentioned, for assessing the hydrokinetic annual energy resource accurately, not only the tidal phenomenon needs to be considered, but also a series of key factors, for instance the freshwater flow or local effects, need to be incorporated within a numerical study, which can be used to assess the resource. Due to the complexity in setting up numerical models and the difficulties in data acquisition for each of the potential regions, it would be rather difficult to have a precise quantification of the available resource considering large geographical regions. Additionally, the variability of the hydrokinetic flow must somehow be assessed for well predicting the net annual harvestable hydrokinetic power [10]. Each area needs to be studied individually and a robust methodology for facilitating the analysis is required. By applying existing standards, a good tidal characterization can be obtained, although, for regions where other effects apart from the tidal flow exist, all stages of procedures should be applied for obtaining consistent results [11,12]. In the case of small to medium-size projects, such an option might not be suitable for a preliminary investigation of the exploitable energy resource.

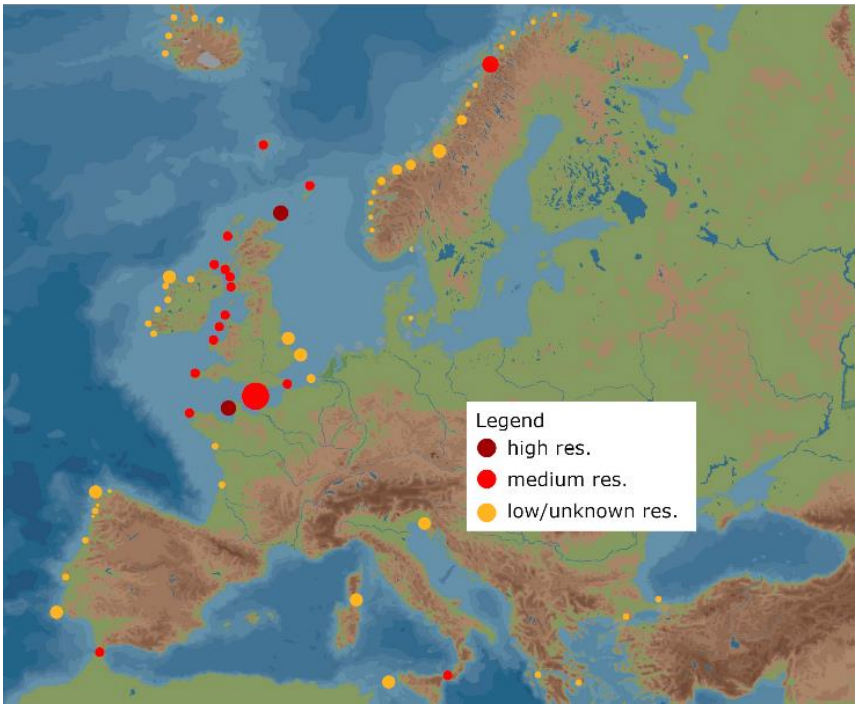

Figure 1. Europe's tidal and hydrokinetic energy hotspots.

Apart from the hydrokinetic energy resource available, it is crucial to investigate several further aspects that may limit the usage of the area of interest [13]. For example, some major constraints can be: (i) installation depth range [14]; (ii) navigational channels and navigational routes [15]; (iii) natural reserve limitations [16]; and (iv) large distance

to the grid connection or energy consumers [17]. While most of the available literature focused on studying the resources in macro-areas, limited studies focused on analysing the hydrokinetic resource in small regions, while taking into account decision-making factors.

Given the aforementioned arguments, the present paper proposes a methodology for analysing the tidal and fluvial hydrokinetic resources for power production in combined estuarine and river regions. Such methodology, compared to typical ones, is tailored for the assessment of limited size waterways having considerable freshwater discharges, shallow waters, and complex morphology. The main objectives of the present work are: (i) to define a methodology for conducting an accurate evaluation of the tidal and river in-stream energy resources in shared estuarine-river areas; (ii) the assessment of the tidal stream and river in-stream energy resources considering the general resource distribution and a high-resolution analysis; (iii) to identify the areas with the highest interest for hydrokinetic energy exploitation and their available resource. Therefore, initially, a methodology is defined (Section 2.1) and then demonstrated for the case study of the Douro waterway (Section 2.2) located in the north of Portugal. Successively, the numerical model developed is explained (Section 2.3), the case study implementation is validated (Section 2.4) and analysis scenarios are described (Section 2.5). Later, the results related to the current speed and kinetic power per cross-sectional area are illustrated (Section 3.1). Successively, the most suitable sites for in-stream turbine deployment are proposed (Sections 3.2 and 3.3) and, finally, concluding remarks are provided (Section 4).

2. Materials and Methods

2.1. Methodology

Tidal and river in-stream energy is typical of coastal regions, where relevant tidal height variations combine with the morphological conditions to produce reasonably fast currents. Consequently, the kinetic energy stored in the water flow can be used for electricity generation, utilizing in-stream Tidal Energy Devices (TEDs), which are installed at the location. In comparison with other forms of renewable energy, the main advantages of tidal and river in-stream energy are: (i) renewable nature and high predictability of the resource; (ii) high load factors associated with tidal currents; and (iii) non-existence of extreme flows that could endanger the long-term survivability of submerged TEDs (i.e., tidal streams velocities rarely exceed 6 m/s).

The kinetic energy of the water flow across a vertical cross-section of a body of water (perpendicularly to the flow direction) per unit time, or in other terms, the power available from the kinetic energy (P_{KE}) of the water flowing through the section, is given by:

$$P_{KE} = \frac{1}{2}\alpha\rho V^3 A \quad (1)$$

where ρ is the water density, V is the magnitude of the water current speed (averaged over the cross-section), A is the surface area of the cross-section (area of action of the rotor), and α is the energy coefficient, defined as:

$$\alpha = \frac{1}{V^3 A}\int_A v^3 dA \quad (2)$$

where v is the magnitude of the current at a generic point of the cross-section. The energy coefficient considers the velocity variations over the water column, being usually set as $\alpha \approx 1$.

For assessing the hydrokinetic power potential of a region of interest, the procedure indicated in Figure 2 (first phase) can be applied. The major steps of the method are: (i) collection of relevant information, (ii) numerical modelling, (iii) numerical validation, and (iv) case study resource assessment. Successively, a second phase can be implemented that focuses on technology selection and detailed economic assessments. For conciseness, the present paper covers only the first phase.

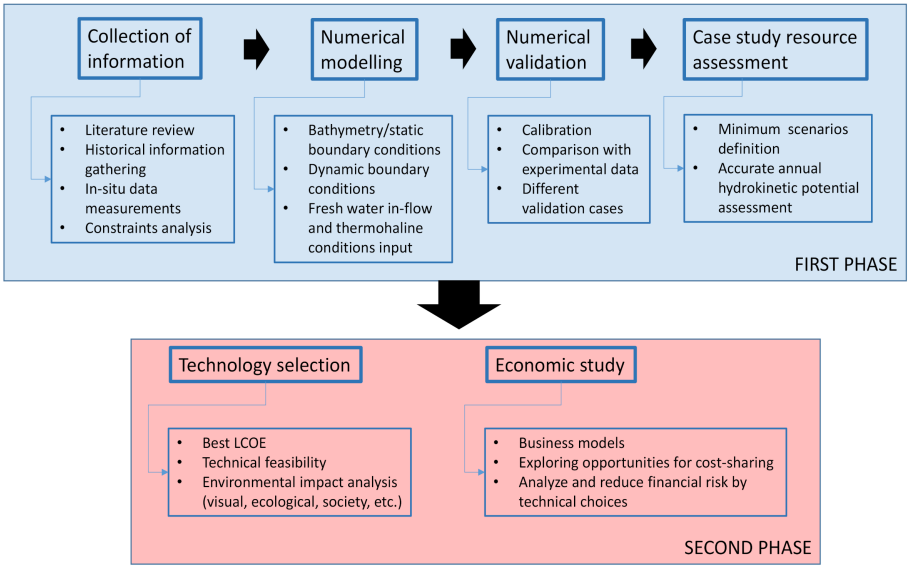

Figure 2. Hydrokinetic power assessment procedure.

A first step towards the goal of investigating the tidal and river in-stream resource is to characterize the water flow throughout the investigated location. For such a scope, two different approaches can be followed: (i) extensive current measurement campaigns and (ii) numerical modelling techniques. The first one consists of gathering velocity measurements at a number of locations during a period long enough to characterize the hydrokinetic energy and its variability induced by the tide (e.g., the spring-neap tidal cycle) and river discharges. The second option involves the implementation of numerical models to simulate the complex hydrodynamics of the estuary. In this case, the numerical models must be calibrated and validated against field measurements so that, after the validation, they can predict the hydrodynamics of the estuary in both space and time with accuracy [18].

In more detail, a high-resolution shallow-water numerical model (e.g., Delft3D-FLOW or MIKE HYDRO river) that simulates the hydrodynamics of the estuary needs to be implemented and validated. Then, to analyse the distribution of the hydrokinetic energy resource, different types of scenarios can be analysed. In this context, there are specific aspects that must be considered for an accurate analysis. In the case of the tidal stream energy resource, a complete mean spring-neap tidal cycle (≈14.75 days) [19] is usually regarded as the period of interest as it shows the most important variability of the tidal currents [20]. However, in the case of the river in-stream resource, an intra-annual analysis of fluvial-induced currents is also mandatory [21]. Given the freshwater discharge regime in the Douro Estuary, the spatial and temporal distribution of the available energy resource can be significantly varying from one time of year to another. Therefore, the intra-annual variability on the river in-stream resource must be analysed by means of a full description of the hydrological regime of the Douro Estuary based on specific periods showing its intra-annual variability. Under this consideration, a preliminary analysis is developed through four characteristic case studies which correspond to a baseline scenario covering a complete mean spring-neap tidal cycle, during which the different seasonal riverine discharges (i.e., spring, summer, autumn, and winter) are considered. The information obtained through these case studies will bring insight into the general patterns of the magnitude and distribution of the hydrokinetic energy resource, along with the influence of the river discharges on the total available resource. Once the general characteristics of the hydrokinetic energy resource are determined, the numerical model is run for a complete year considering mean monthly river discharges in order to compute accurately the total resource available along with other parameters of interest [15].

Finally, the so-called Tidal Stream Exploitability (TSE) index [14], adapted to the characteristics of the estuary, can be applied. Such an index includes a penalty function and parameters related to the flow velocity and water depth. Based on the TSE value, the areas of interest for hydrokinetic energy exploitation are selected and retained for further analysis through high-resolution techniques. To study the general resource distribution, in the first place, an intra-annual analysis should be conducted. Various scenarios, showing the intra-annual variability of riverine discharges under the tidal action, should be analysed to determine the variability that they impose on the total hydrokinetic resource. This information can be obtained by superimposing a complete mean spring-neap tidal cycle (as a representative period of the fortnightly inequality of the tide) and the mean seasonal discharges. In order to have a full description of the combined effects of both components of the hydrokinetic resource (i.e., tides and fluvial discharges) and to obtain accurate mean annual figures, an annual scenario is also simulated for a long period. To select the areas of highest interest for energy exploitation, the TSE index adapted to the characteristics of the estuary is then computed as described in [14]:

$$TSE = \frac{\xi}{2V_0^3 h_0}\left(V_f^3 + V_e^3\right)h_m \quad (3)$$

where ξ is the penalty function, V_0 and h_0 are the characteristic velocity and water depth, V_f and V_e represent the depth-mean velocities at mid-flood and mid-ebb, and h_m is the mean water depth.

In consequence, the delimitation of the areas suitable for hydrokinetic energy exploitation is carried out using the TSE index. Typical values of TSE indicating good tidal resources are in the range 1 to 5 or above [14]. Within these areas, the most adequate locations are selected for further analysis, and the available resource is analyzed in detail by considering a complete-neap tidal cycle under mean river discharges.

2.2. Case Study Region Characteristics

To have a holistic understanding of the case study, it is important to outline the region of interest also taking into consideration diverse features, such as physical, operational, and climatic characteristics. For instance, the Douro River flows from its source in the peaks of the Urbión mountain, in the Spanish province of Sória, at 2160 m of altitude, to the Atlantic Ocean in Porto. It crosses the North of Portugal in Barca de Alva, stretching around 900 km from its source to its mouth (Foz do Douro) located between the cities of Porto and Vila Nova de Gaia (Figure 3).

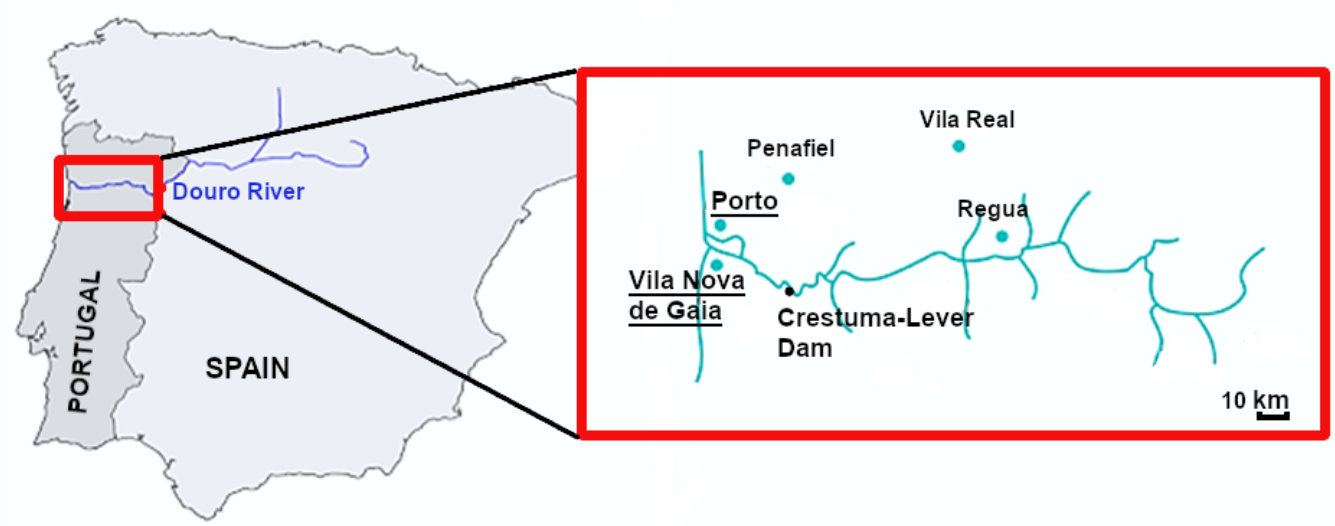

Figure 3. Douro Estuary and Douro River.

The River Douro is the second largest river in Portugal, spanning a total length of 208 km in Portugal and presenting a basin of 18,643 km^2 with a vertical gap of 125 m, which comprehends 5 navigation locks (from 13 to 35 m in height). The Port Authority of Douro, Leixões and Viana do Castelo (APDL, SA) manages the inland waterway of the Douro River (in Portugal). The waterway is open, all along its Portuguese extension, to recreational boats (except sailboats with over 7.20 m of mast). In this context, the River Douro waterway is an important touristic route in Portugal, having received over 1.2 million passengers from cruise ships and recreational vessels in 2018. In 2018, cargo traffic reached 33,829 tons, an increase of 7% from 2016. Based on annual figures of energy consumption alongside Douro's waterway (approx. 1 GWh/year and the consequent CO_2 emissions of ca. 233 tons), APDL has the opportunity to reduce its carbon footprint and improve its renewable energy capacity by exploiting the resource associated with the streams caused by the combination of the tides and river runoffs.

The hydrodynamic behaviour of the estuary is governed by the complex and non-linear combination of different coastal processes (forcing factors), such as tides, waves, river runoffs, wind, salinity, and temperature gradients. On the one hand, the river mouth area presents highly energetic wave and tidal regimes. The wave regime presents an NW-W predominant direction, inducing a drift current in the N-S direction that is reversed at the estuary mouth. This situation is responsible for the presence of a sand spit, which is associated to seasonal dynamics [22]. The tidal regime presents a semi-diurnal behaviour with a period of 12.4 h. Additionally, the tidal range varies from 2 to 4 m. Spring tides produce elevations of 2.8 m (in relation to the Mean Sea Level, MSL) at the mouth and 2.6 m (MSL) at the head of the estuary, with a 1 h lag between them. In consequence, significant tidal prisms are present in the area, ranging from 10×10^6 m^3 to 25×10^6 m^3 for neap and spring tides, respectively [22]. On the other hand, freshwater runoffs are governed by the Crestuma-Lever dam, which is located about 18 km upstream from the river mouth. Precisely, mostly in the upper section of the estuary, the hydrodynamics are mainly ruled by the freshwater discharges of the dam. In some cases, flow rates exceed 13,000 m^3/s. Furthermore, freshwater runoffs present a considerable inter-annual variability [23], associated with the dry and rainy years. In consequence, rainy years may result in torrential regimes, resulting in strong flow currents and flooding events. Therefore, for strong flow rates (exceeding 800 m^3/s), the riverine water is flushed to the sea and seawater intrusion is prevented during flooding. For low river discharges (e.g., <300 m^3/s), the ocean water enters the estuarine region with a salt wedge configuration. As a result, the freshwater residence time varies from 8 h to more than 2 weeks depending on the river flow [22].

Concerning the bathymetric characteristics, the area of study presents an irregular bathymetry with water depths up to 28 m, however, water depths are generally in the range of 0 and 10 m (Figure 4).

2.3. Numerical Modelling Implementation

As it has been previously defined, the first step towards the assessment of the hydrokinetic in-stream energy resource is a full description of the hydrodynamics of the area of interest. With this aim, for demonstration, a Delft3D-FLOW high-resolution shallow-water numerical model was defined and subsequently validated within the Douro Estuary. This numerical model can be implemented either as a 3D model or in its 2DH form (vertically averaged), being the last option selected for this work, as in the case of several other hydrokinetic resource assessments [18,20,21,24]. A number of implementations of Delft3D-FLOW were conducted to determine: (i) the general resource distribution and (ii) a high-resolution analysis of the areas of interest. Delft3D-FLOW is a finite difference code that solves the Navier-Stokes equations (under the shallow-water and Boussinesq assumptions) along with the transport equation, thereby allowing the computation of both the barotropic and baroclinic circulation [25]. The computation of baroclinic circulation, which considers the flow driven by horizontal density gradients, can be of paramount

importance in the case of semi-enclosed water bodies (e.g., estuarine areas), where riverine and ocean water mix occurs. The model equations in their 2DH form are:

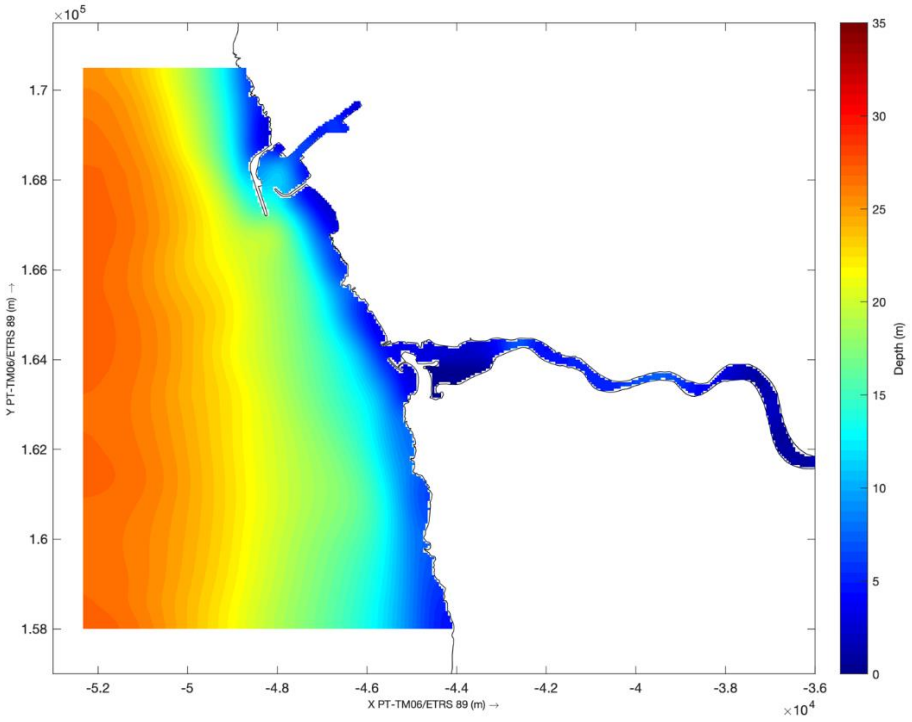

Figure 4. Bathymetry interpolated to the Cartesian grid.

$$\frac{\partial \zeta}{\partial t} + \frac{\partial[(d+\zeta)U]}{\partial x} + \frac{\partial[(d+\zeta)V]}{\partial y} = Q \tag{4}$$

$$\left.\begin{aligned} \frac{\partial U}{\partial t} + U\frac{\partial U}{\partial x} + V\frac{\partial U}{\partial y} - fV &= -g\frac{\partial \zeta}{\partial x} - \frac{g}{\rho_0}\int_{-d}^{\zeta}\frac{\partial \rho'}{\partial x}dz + \frac{\tau_{sx}-\tau_{bx}}{\rho_0(d+\zeta)} - v_h\nabla^2 U \\ \frac{\partial V}{\partial t} + U\frac{\partial V}{\partial x} + V\frac{\partial V}{\partial y} + fU &= -g\frac{\partial \zeta}{\partial y} - \frac{g}{\rho_0}\int_{-d}^{\zeta}\frac{\partial \rho'}{\partial y}dz + \frac{\tau_{sy}-\tau_{by}}{\rho_0(d+\zeta)} - v_h\nabla^2 V \end{aligned}\right\} \tag{5}$$

$$\frac{\partial(\zeta+d)c}{\partial t} + \frac{\partial[(\zeta+d)Uc]}{\partial x} + \frac{\partial[(\zeta+d)Vc]}{\partial y} = D_h\nabla^2 c - \lambda_d(d+\zeta)c + R \tag{6}$$

Equation (4) expresses the conservation of mass under the assumption of incompressibility (Boussinesq assumption); Equation (5) represents the conservation of the momentum along x- and y- directions; and finally, Equation (6) is the transport equation, which is solved for both temperature and salinity. In these equations, d and ζ stand for the water depth and water level (both relative to a reference plane); U and V are the vertically integrated eastward and northward components of the velocity; ρ' and ρ_0 express the anomaly density and reference density of the seawater; f is the Coriolis parameter; Q stands for the intensity of mass sources; v_h expresses the horizontal eddy viscosity; τ_{bx} and τ_{by} are the shear stress components at the sea bottom; τ_{sx} and τ_{sy} are the wind stress components acting on the sea surface; c stands for the temperature or salinity constituents; D_h is the horizontal eddy diffusivity; R is for the source term per unit area; and finally, λ_d represents the decay processes of the first-order.

Regarding the spatial discretisation, the model used the so-called Arakawa-C grid, a staggered grid by which the water levels ζ are computed at the central points of the grid faces, whereas the flow velocity components (U and V) are defined at the central points of the grid faces, to which they are perpendicular [26]. Moreover, the horizontal advection terms in Equations (4) and (5) are dishwater discretised by using the Cyclic method [27].

Finally, temporal discretisation was carried out by Delft3D-FLOW through a semi-implicit ADI (Alternating Direction Implicit) algorithm with two-time levels per iteration [28].

Several forcing factors should be used as input to the numerical model. On the one hand, for the water level variation along the ocean boundary, a Dirichlet boundary condition was imposed (i.e., the sea level was prescribed as a function of time). By such approach, the major tidal harmonics (A0, M2, S2, N2, K2, K1, O1, P1, Q1, MF, MM, M4, MS4, and MN4) obtained from the database TPXO 7.2—a global model of ocean tides that solves the Laplace equations using data from tide gauges and the TOPEX/Poseidon Satellite [29,30]—were used. A full list of the adopted harmonics for the study region is provided in Appendix A. The number of harmonic constituents chosen ensured that more than 99% of the tide amplitude was accounted for. A spatially varying method was used, in which the tidal harmonics were extracted for each open boundary of the model. In the case of estuarine areas, a part of the tidal force's other driving agents are responsible for inducing hydrokinetic currents and they must be accurately analysed [21]: (i) fluvial discharges and (ii) thermohaline conditions. Data of freshwater discharges was obtained from the flow rates measured at the Crestuma-Lever dam, which consisted of hourly flow rates from the year 1990 to 2018. Later, Table 2 presents the main statistical characteristics of the flow data, summarising the mean seasonal figures of fluvial discharges (in terms of flow rate and water temperature) for the area of study. For the thermohaline conditions, a constant salinity and temperature distribution was prescribed along the ocean boundaries. According to previous studies on the region [31,32], salinity was set to 35.8 ppt, whereas temperature was set to 18 °C. Finally, additional forcing factors were also considered during the implementation of the model: (i) the Coriolis factor, with a value of 9.56×10^{-4} s^{-1}, was adopted by using the mean latitude value of 41.10° N of the study area; and (ii) for the bottom roughness, the Manning formulation was adopted by using a Manning roughness coefficient (n) of 0.039 $sm^{0.33}$.

For the case study region, the numerical model grid covered the stretch of the estuary from the Crestuma-Lever barrage to Foz do Douro (estuary mouth) and extended towards the adjacent continental shelf roughly up to the 40 m isobath, enough to ensure that possible numerical disturbances at the boundaries did not affect the model results in the area of interest. The developed grid was composed of varying-size cells, with the grid size set as follows: in the inner and middle estuary, a grid resolution of 50 × 50 m was adopted, which linearly decreased from the outer estuary up to 200 × 50 m at the ocean boundary of the grid. The model was run with a time step of 30 s, which according to the Courant–Friedrichs–Levy criterion (the so-called CFL condition), was sufficient to ensure numerical stability considering the resolution adopted for the finite-difference mesh [20]. The bathymetric data was obtained from the Bathymetric model of Douro, IH Portugal. In addition, the bathymetry of the Port of Leixões was supplemented by the detailed bathymetric dataset provided by the port authority–APDL. Finally, both datasets were interpolated onto the computational domain of the model with the aid of the Delft3D-QUICKIN toolbox.

The initial conditions for the hydrodynamic numerical model were based on the so-called cold start, i.e., zero free surface elevation and water velocity throughout the computational domain [33]. Regarding the transport model, the initial thermohaline conditions (i.e., salinity and temperature) were prescribed at the oceanic open boundaries by means of field measurements. Moreover, in order to ensure that the cold start could not affect the numerical results, the model was run through a spin-up period [34,35] of 15 days (model time) before the period of interest of the numerical simulations during which the results were analysed.

For the boundary conditions, a Dirichlet boundary condition was imposed along the oceanic boundaries by means of the main tidal constituents of the astronomical tide and the thermohaline conditions. Since the length of these boundaries is two orders of magnitude smaller than the length of the tidal wave, the phase of the tidal constituents was assumed to be constant along the oceanic boundary [33]. At the land-water transition, null flow

through the boundary and the free slip condition (i.e., zero shear stress) was imposed. On the contrary, at the sea bottom boundary, the seabed shear stress was computed from:

$$\begin{aligned} \tau_{bx} &= \frac{1}{C_{2D}^2}\rho_0 g U\sqrt{U^2+V^2} \\ \tau_{by} &= \frac{1}{C_{2D}^2}\rho_0 g V\sqrt{U^2+V^2} \end{aligned} \quad (7)$$

where C_{2D} represents the Chézy coefficient, highly dependent on the bottom roughness and water depth. This dependency can be expressed by means of the Manning coefficient: n:

$$C_{2D} = \frac{\sqrt[6]{d+\zeta}}{n} \quad (8)$$

In this work, given that the average water depth in Douro Estuary (≈16 m) is well above 10 m, a constant value of 0.015 was adopted for the Manning coefficient [36].

The surface stress due to the wind action is given by:

$$\vec{\tau}_s = \rho_a C_D \left|\vec{U}_{10}\right| \vec{U}_{10} \quad (9)$$

where ρ_a represents the air density, U_{10} stands for the wind velocity vector at 10 m height above the sea surface, and C_D is the dimensionless wind drag coefficient, which is usually modelled by the following expressions [37,38]:

$$\left.\begin{aligned} C_D &= 1.1\times 10^{-3} && \text{for } U_{10} < 6\ \text{ms}^{-1} \\ C_D &= (0.50+0.071U_{10})\times 10^{-3} && \text{for } U_{10} \geq 6\ \text{ms}^{-1} \end{aligned}\right\} \quad (10)$$

2.4. Model Validation, Calibration and Analysis

To ensure that the model accuracy is sufficient to realistically solve the hydrodynamic conditions of the region of study, the model was validated against field data of water level variation and flow velocities. The validation period covered from 19 September to 5 October 1994, during which a hydro-morphological campaign was carried out in the Douro Estuary [23,39]. Tidal elevations, currents, among other variables, were sampled at several points, which were distributed horizontally among the region and vertically at three different depth heights. Water level variations were recorded at three stations placed in Cais da Estiva (WL1 in Figure 5), Port of Leixões (WL2 in Figure 5), and Cantareira (WL3 in Figure 5). Table 1 shows the exact location of each station.

Table 1. Location of the validation points (coordinate system: PT-TM06/ETRS89).

Station	X-Coordinate (m)	Y-Coordinate (m)
WL1	−40327.66	163549.96
WL2	−48118.66	168627.78
WL3	−44801.62	164280.92

For the calibration of the model, different values of v_{Hback} and D_{Hback} (5, 10, 25 and 20 m^2/s) were used. The performance of the different calibration values can be assessed against water level variations (WL1, WL2, and WL3). As an example, Figure 6 shows the calibration results with their respective statistical parameters (Correlation Coefficient, R^2 and Root Mean Square Error, RMSE).

As can be observed in Figure 6, the best validation results were obtained for the values of 10 m^2/s for both v_{Hback} and D_{Hback}. Therefore, those values were retained for implementation in the model. For the same validation tests, time-series (for a period of 4 days) of the water level are illustrated in Figure 7. Major differences (up to about 0.3 m) between measured and numerical values were observed at low and high tides at Station

WL1. Such differences may be due to local effects at Station WL1, which are not fully captured by the numerical model.

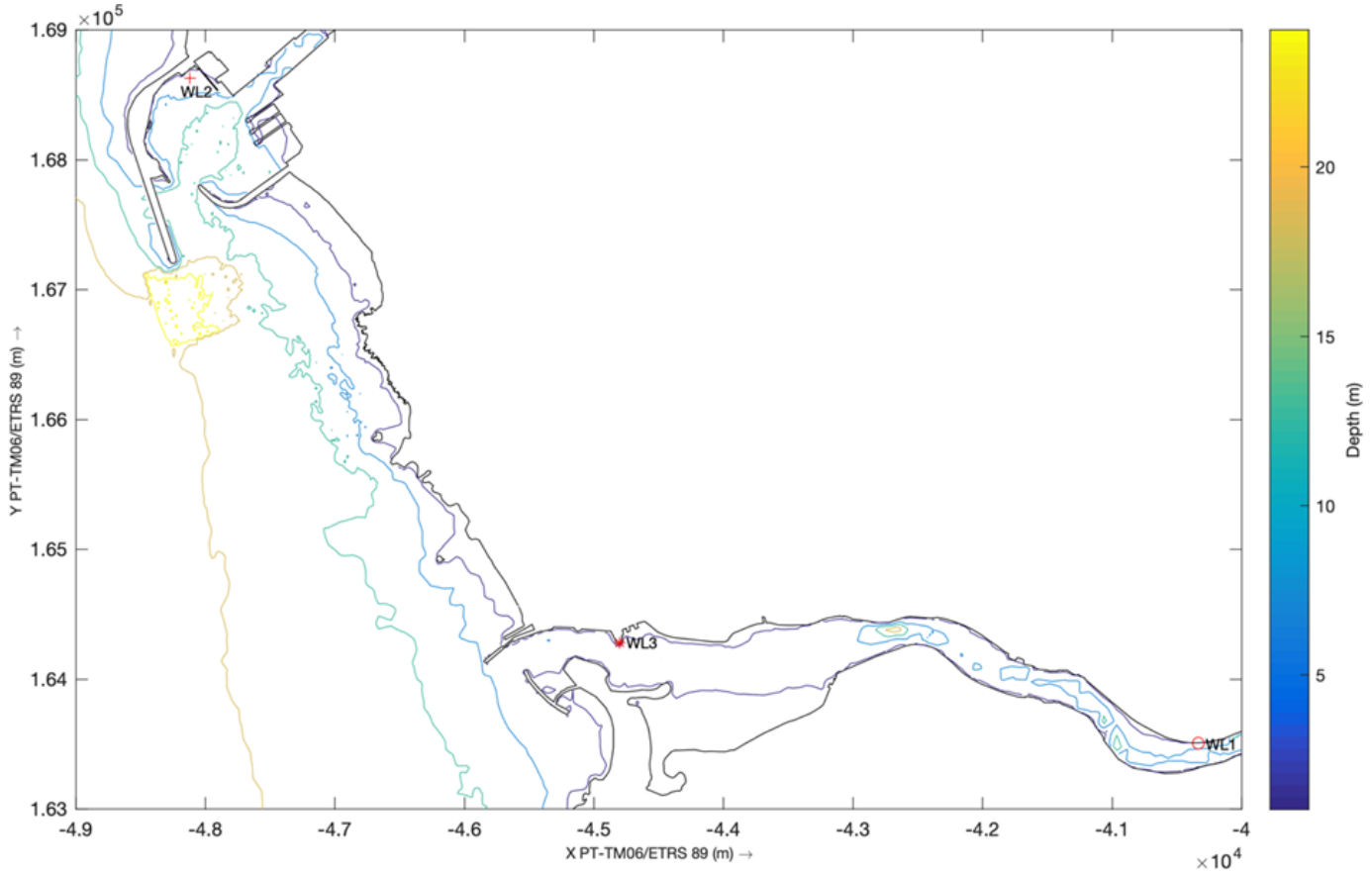

Figure 5. Location of the tidal gauges and ADCPs.

2.5. Scenarios Analysed

For a preliminary analysis of the hydrokinetic energy resource distribution resulting from the combined action of the tide and river discharges, a complete mean spring-neap tidal cycle (≈14.75 days) should be analysed. During this period, seasonal river discharges (Table 2) are input into the model by setting four scenarios (S1–S4) (Table 3).

Table 2. Fluvial discharges of the Douro Estuary (from Crestuma-Lever to Foz do Douro).

Season	Mean Season Discharges (m^3/s)
Spring	284.13
Summer	185.48
Autumn	764.3
Winter	833.1
Mean	512.26

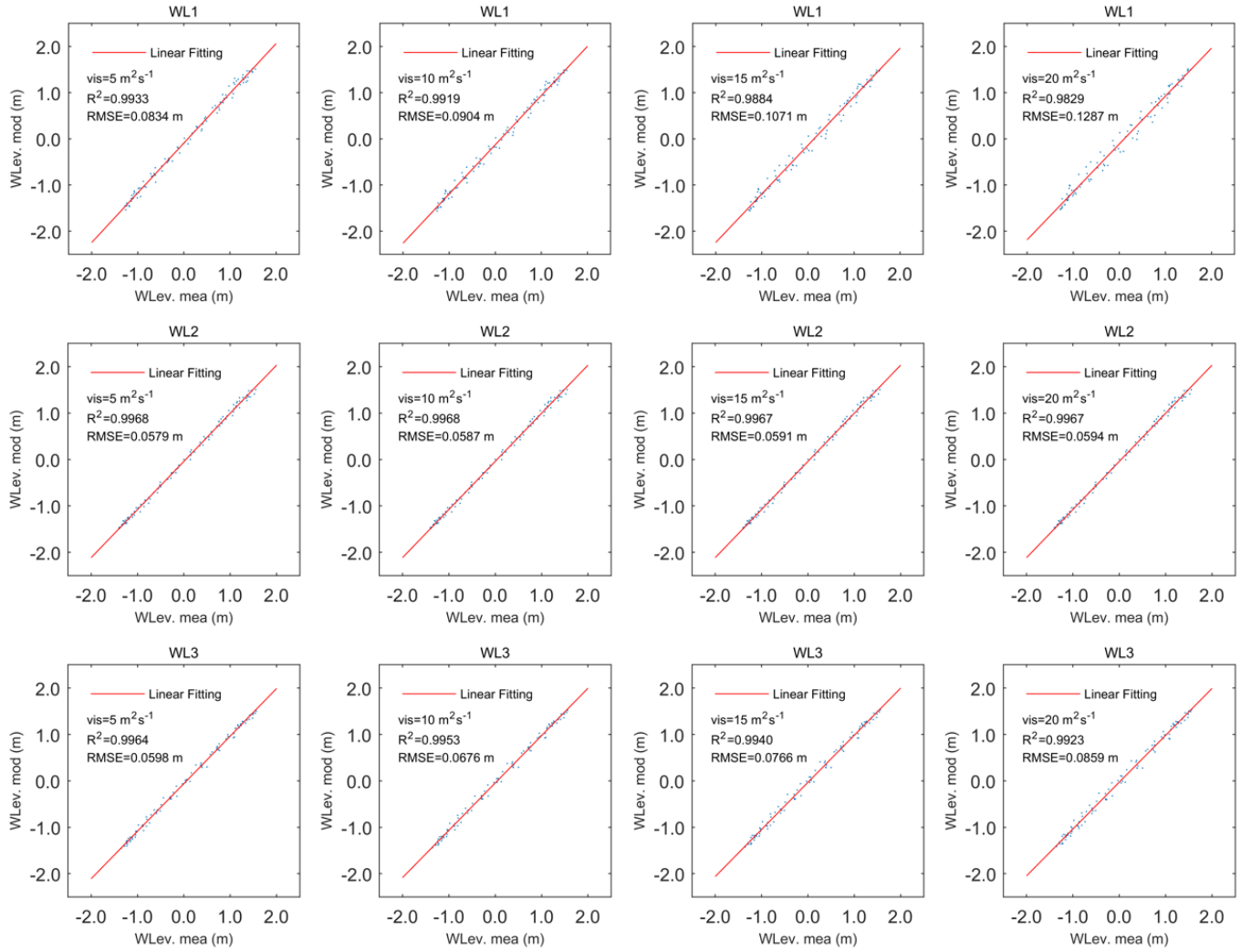

Figure 6. Model calibration results.

Table 3. Definition of scenarios.

Time Period	River Discharges	Objective	ID
Complete mean spring-neap tidal cycle	Winter *	General resource distribution analysis	S1
	Spring *		S2
	Summer *		S3
	Autumn *		S4
Annual scenario	Monthly mean	Mean power density, energy production and performance	S5
Tidal cycle (spring tide)	Mean	TSE index	S6
Complete mean spring-neap tidal cycle	Mean	High-resolution analysis	S7

* Corresponding fluvial discharges are reported in Table 2.

In order to study the combined effects of both energy resources over a long time and to determine with accuracy the total energy resource available, a complete year should be also simulated, during which the numerical model is forced with mean river discharges (S5). Then, the spatial distribution of the TSE index is determined by considering a tidal cycle during spring tides under mean river discharges (S6). Finally, in the light of the results obtained, the temporal distribution of the resource available is analysed at the locations selected by considering a complete-neap tidal cycle under mean river discharges (S7). Table 3 summarizes the definition of the different cases studies simulated in this work.

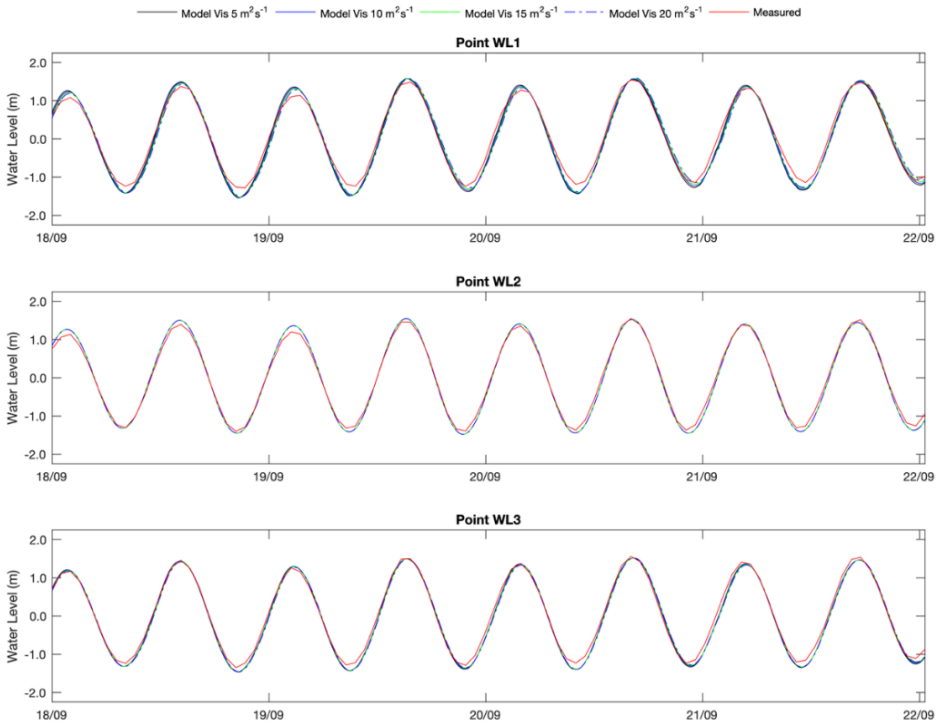

Figure 7. Time-series of water elevation validation results in points WL1, WL2, and WL3.

3. Results and Discussion

3.1. General Resource Distribution

In this section, the general distribution of the combined tidal and river in-stream energy resource along the Douro Estuary is analysed in detail. The results obtained from S1 to S4 (Table 3), which show the flow velocity magnitude throughout the Douro Estuary at mid-ebb and mid-flood of a mean spring tide, are presented in Figures 8–12.

As can be observed in Figure 8, for S1 (i.e., using winter river discharges of 833.10 m^3/s during a mean spring tide), significantly stronger currents occurred at mid-ebb. This characteristic occurred since the driving forces of the flow (river discharges and tide) were applied in the same direction. In this case, flow velocities that easily exceeded 1.25 m/s at the mouth of the estuary were observed. Furthermore, in the inner part of the estuary where the effect of the river discharge is predominant, multiple locations presented flow velocities in the order of 1 m/s. Conversely, at mid-flood, the flow velocities at the estuary mouth were significantly lower, since the direction of the flow driven by the tide opposed the flow driven by the river discharges. In the inner estuary, the behaviour is similar to the mid-ebb scenario.

Figure 9 shows the results obtained for S2 (i.e., using river discharges relative to the spring season of 284.13 m^3/s during a mean spring tide). Similar to S1, stronger currents occurred at mid-ebb, in which values up to 1.25 m/s were observed at the mouth of the estuary. In comparison with S1, the significantly lower river discharge resulted in weaker currents in the inner estuary, with most of the points presenting flow velocities well under 0.5 m/s. It is worth noting that at mid-flood flow, the effects of the lower river discharge (in comparison with S1) resulted in velocities in the order of 0.5 m/s at the mouth of the estuary since the opposing force caused by the river discharges was significantly lower. Based on these results, a velocity asymmetry was apparent with significant greater velocities during the ebb, or ebb dominance, which in part may be determined by the river discharges. More specifically, despite the tidal range of the area (ca. 3 m), the general circulation behaviour appeared to be dominated by the river runoffs.

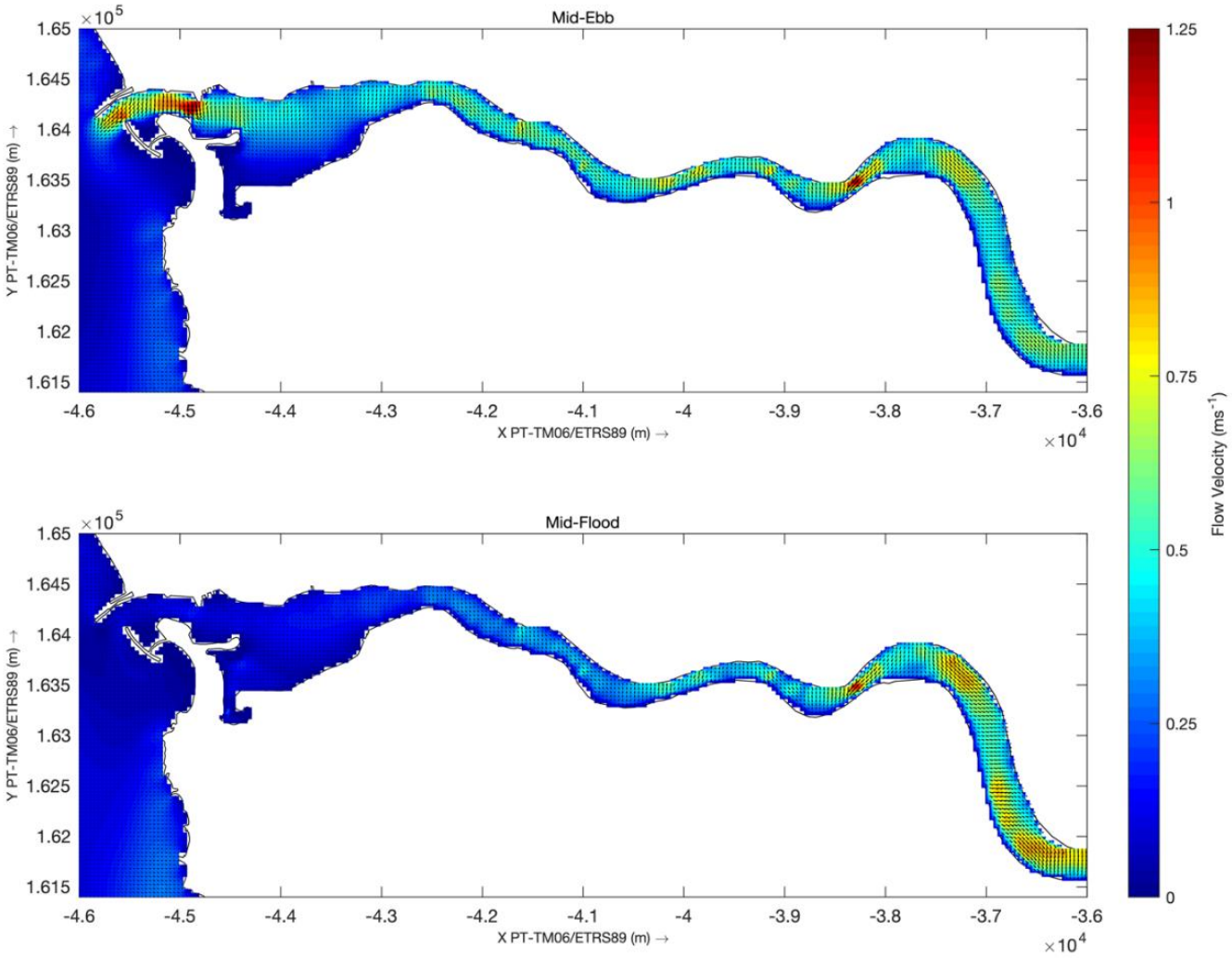

Figure 8. Flow velocity magnitude at mid-ebb (**up**) and mid-flood (**down**) for scenario S1.

For S3 (Figure 10) and S4 (Figure 11), the flow presented a similar behaviour to S2 and S1, respectively.

Once the seasonal hydrodynamic pattern of the estuary is analysed, the mean annual velocity and power density in the estuary can be determined (Figures 12 and 13, respectively). For this purpose, the hydrodynamics of the estuary were computed for a complete year, in which river discharges were input into the model on a monthly basis (Figure 12). Then, for each point, the flow velocity was averaged taking into consideration every time step of the simulation.

Figure 12 shows the mean annual velocity in the estuary. As expected, three different areas of interest can be highlighted. On the one hand, in the inner estuary, the flow velocities were between 0.5 and 0.8 m/s, which were highly influenced by the river discharges. On the other hand, at the mouth of the estuary, two areas stand out with mean flow velocities in the order of 0.75 m/s.

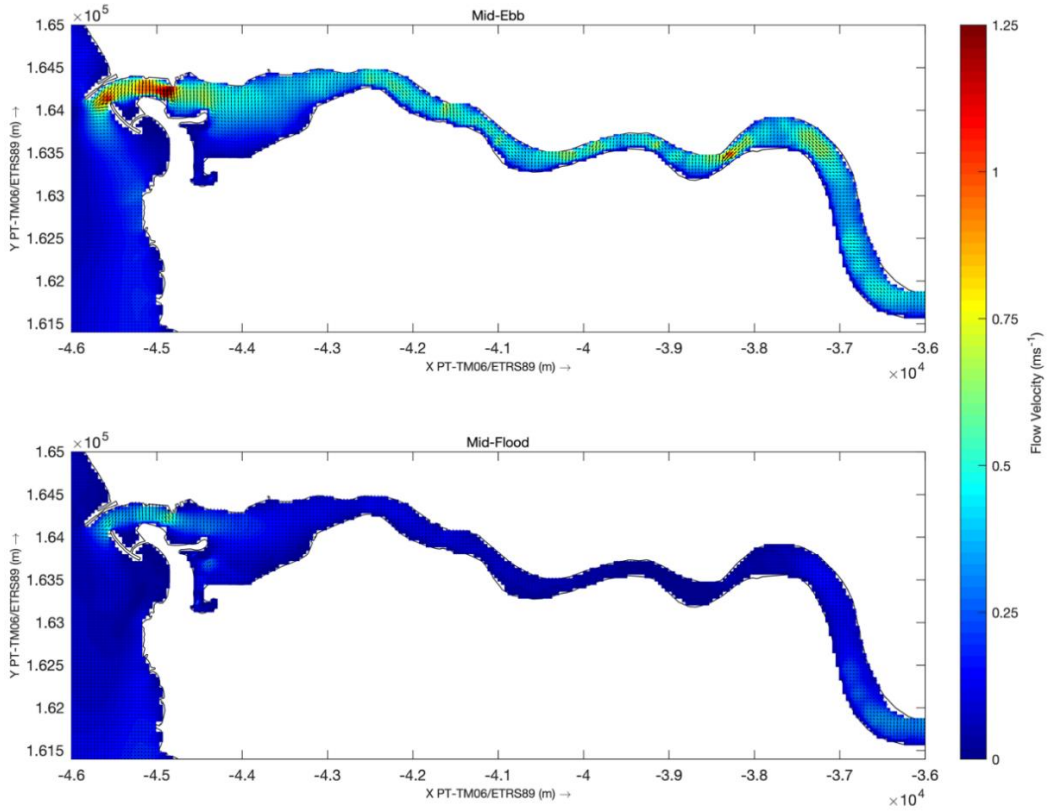

Figure 9. Flow velocity magnitude at mid-ebb (**up**) and mid-flood (**down**) for the scenario S2.

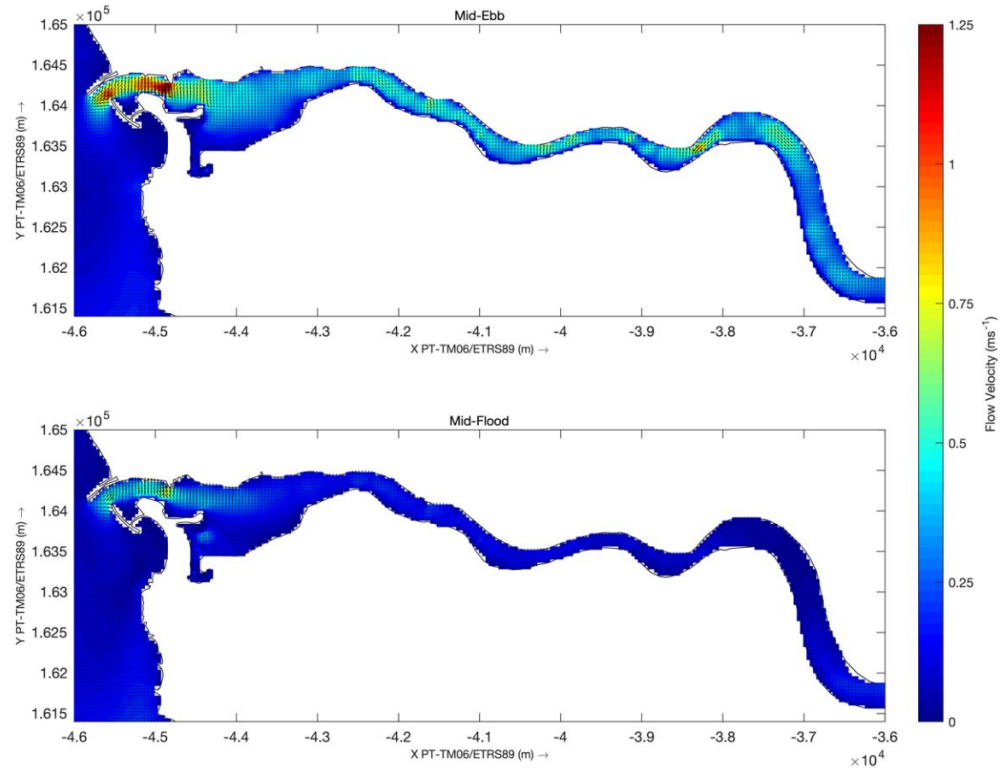

Figure 10. Flow velocity magnitude at mid-ebb (**up**) and mid-flood (**down**) for scenario S3.

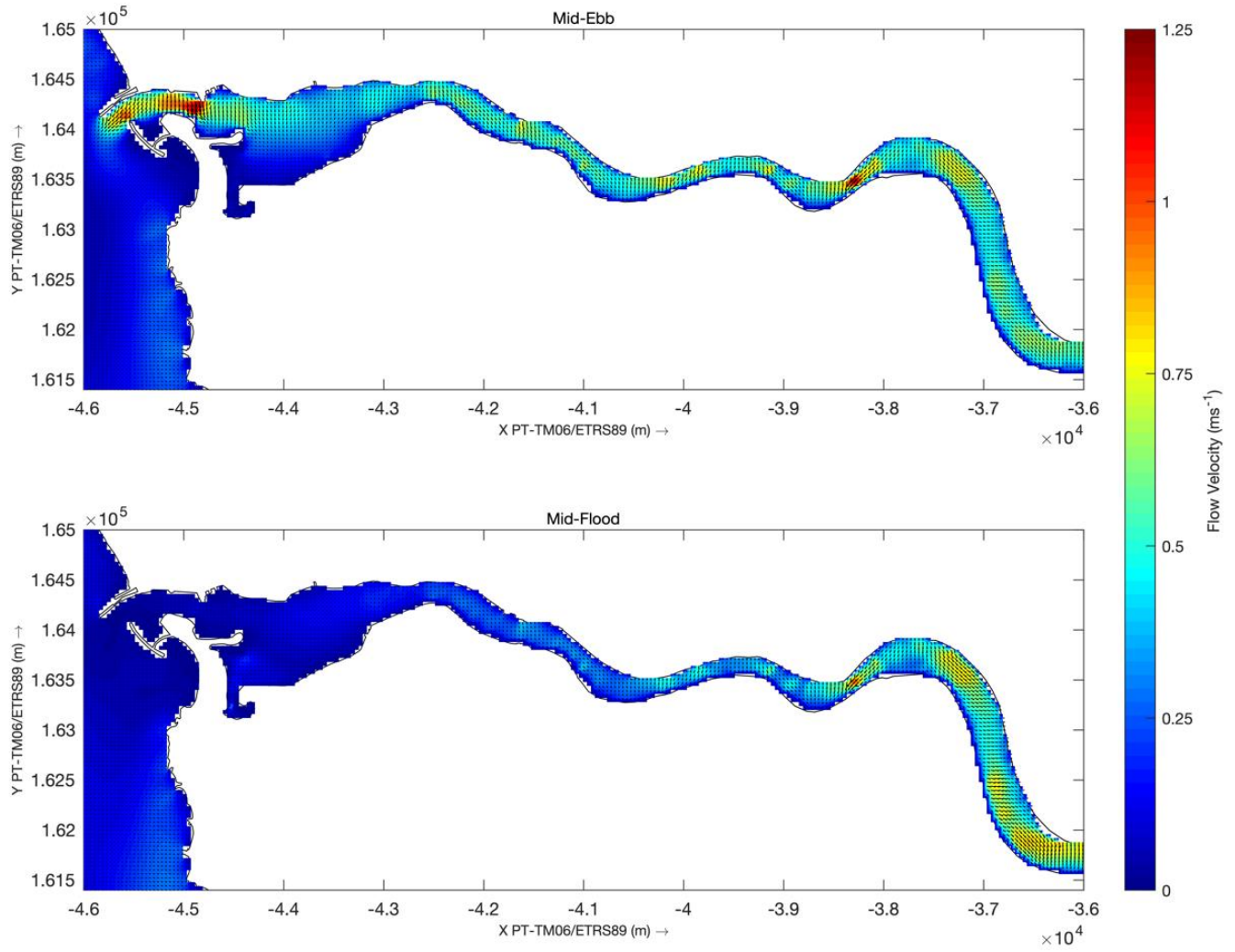

Figure 11. Flow velocity magnitude at mid-ebb (**up**) and mid-flood (**down**) for scenario S4.

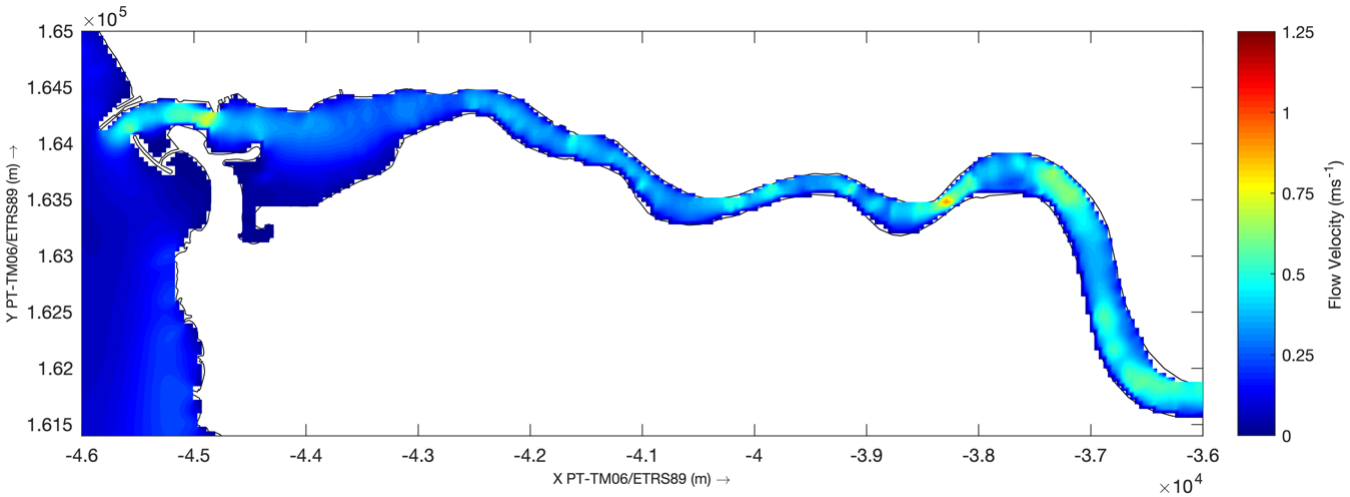

Figure 12. Mean annual flow velocity (assuming mean monthly river discharges).

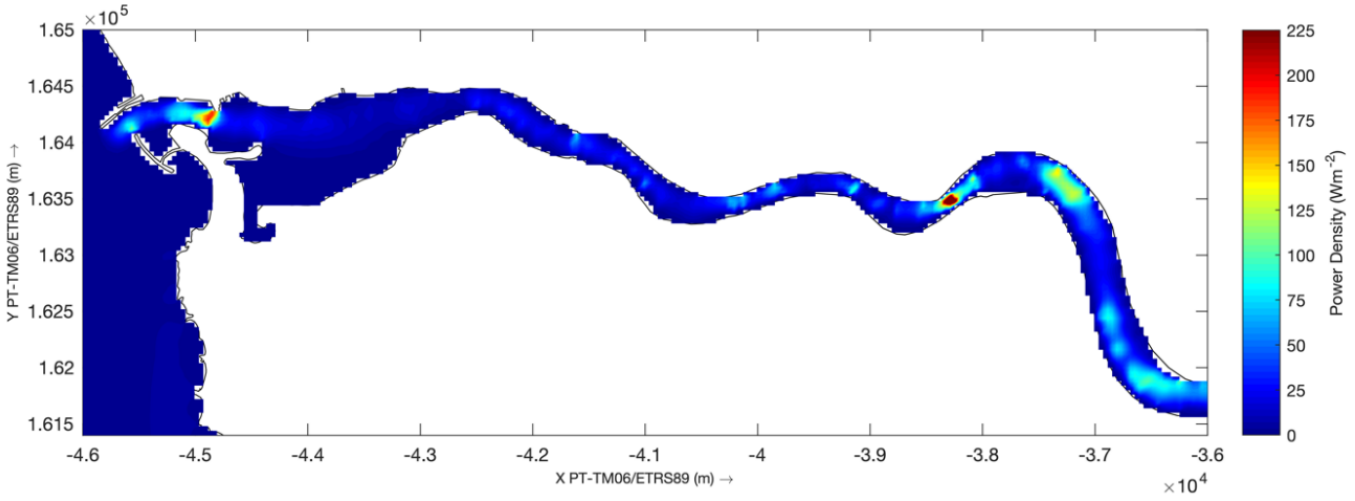

Figure 13. Mean annual power density (assuming mean monthly river discharges).

Figure 13 shows the mean annual power density of the estuary. As can be observed, three areas, with two of them located in the inner estuary and the other one at the river mouth, could potentially be exploited, since they present mean annual power densities that close to 0.4 kW/m^2. However, for depth-limited regions such as the Douro Estuary, the available water depth plays a major role in the selection of potential tidal sites. To account for these potential limitations, the spatial distribution of the TSE index was computed for the estuary according to Equation (3). For the present study, the TSE index was computed throughout the estuary for S6 by considering the mean annual values of fluvial discharges (Figure 12). Furthermore, according to the characteristics of the Douro Estuary, the values for the characteristic velocity (V_0) and water depth (h_0) were set to 0.5 m/s and 6 m, respectively. These values were adopted based on figures provided by Fertahi [40] and taking into consideration available water depths. However, it has to be pointed out that the mentioned values may vary based on other specific TEDs considered [20]. For the scope of this study, generic TEDs, that satisfy the adopted V_0 and h_0, were consequently assumed.

As can be observed in Figure 14, the TSE index limited the number of potential tidal sites, being these are mainly limited to the inner estuary, in which the TSE index values reached up to 2.8. In consequence, the areas with the highest potential were analysed in detail by assessing the time-series distribution of the flow velocity and power density, using for this purpose a complete-neap tidal cycle under mean river discharges.

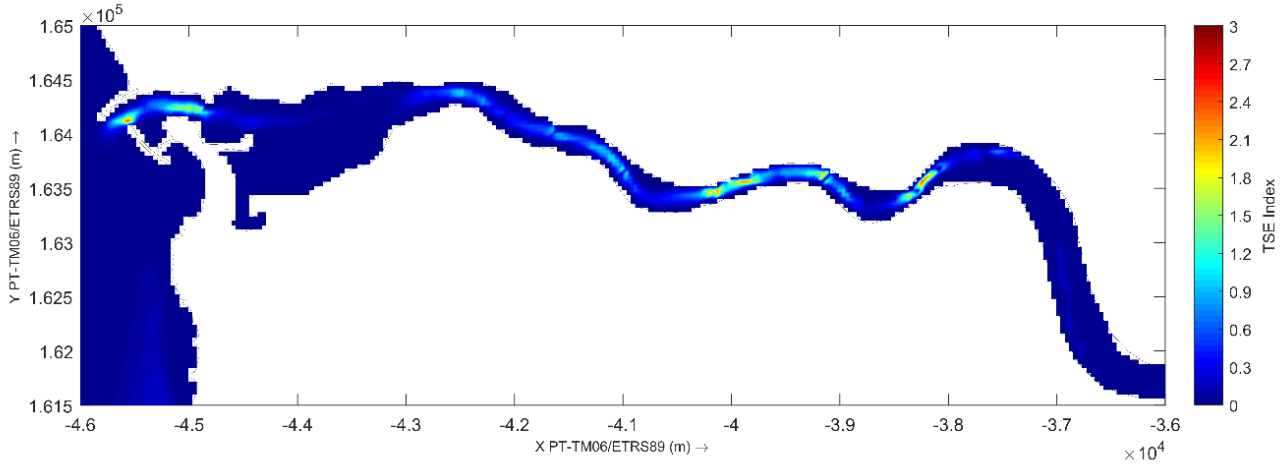

Figure 14. TSE index for the Douro Estuary.

3.2. Selection of Sites

Four areas (A to D) throughout the Douro Estuary were identified as of potential interest for tidal and river in-stream energy exploitation based on the results of the Tidal Stream Exploitability (TSE) index [14]. Table 4 summarizes the main characteristics of the areas identified through the site selection procedure. Indicative locations of these areas are illustrated in Figure 15.

Table 4. Main characteristics of hydrokinetic selected sites.

Area	Indicative Total Surface (m^2)	Feasible Surface (m^2)	Seabed Classification	Mean Water Depth (m)	Maximum TSE
A	21000	7404	Gravel	7	2.2
B	8000	5163	Gravel	6.7	2.3
C	18000	2011	Gravel	8.1	2.1
D	22000	4797	Gravel	6.2	2.8

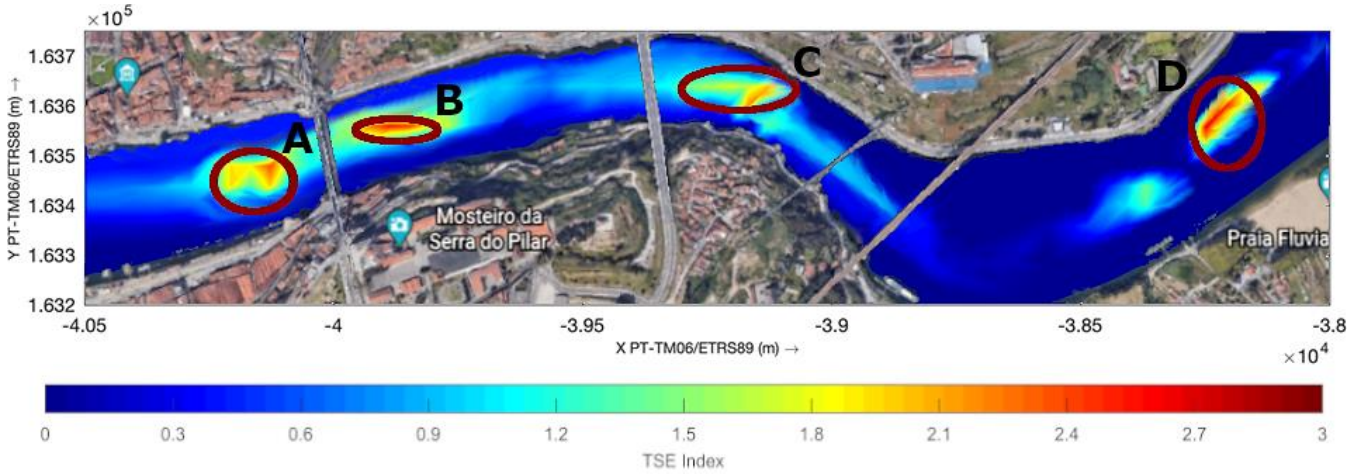

Figure 15. Location and TSE index values for the suitable exploitation areas.

The initial stage of the site selection only considers the energy availability along with the water depth. Therefore, to conduct an integrated site selection, additional environmental and socioeconomic aspects should be analysed also considering the different marine uses within the Douro Estuary. For instance, the size of the navigation channel was considered so far in this work (Figure 16). Further details should be covered in the later SWOT analysis.

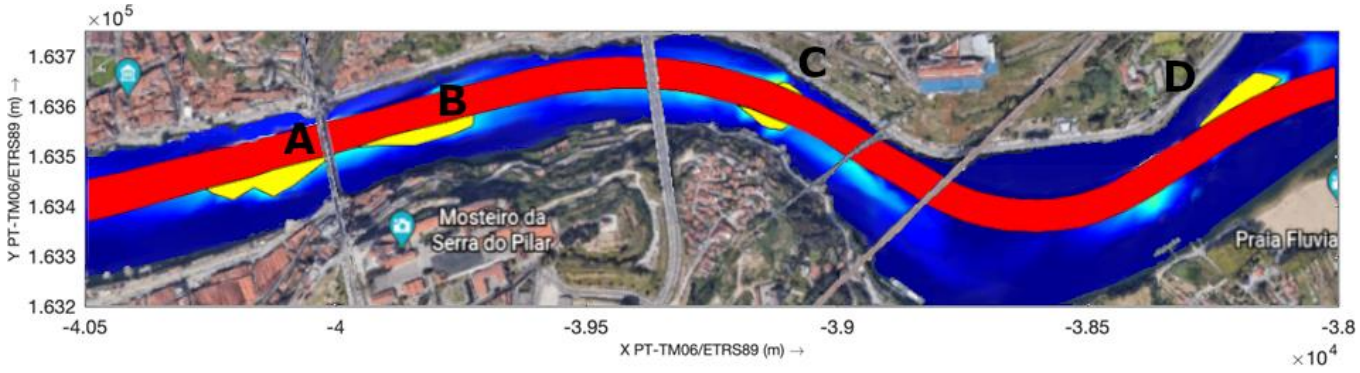

Figure 16. Exploitable surface for Areas A, B, C, and D (Yellow) and restricted area of the navigation channel (Red).

From the superimposition of the selected areas, based on the TSE index, and the restricted area of the navigation channel, the resulting sites of interest for the hydrokinetic

energy exploitation, i.e., those that do not fall within the navigation channel, are presented in Figure 16. As it can be observed, all the areas identified are partially (or almost completely, as in the case of Area C) located within the restricted area of the navigation channel. Thus, given the information made available, it can be established that only a limited surface (feasible surface) would satisfy the requirements for integrated hydrokinetic energy exploitation (Table 4), determined by the available resource and factors related to other marine uses.

3.3. High-Resolution Analysis of Areas of Interest

The most representative locations of the previously selected areas need to be analysed in detail. Therefore, the flow velocity at the locations corresponding with the maximum value of the TSE index, within the areas of interest (Table 4), is analysed in terms of eastward and northward components and flow magnitude.

Detailed results for Areas A to C are provided in Appendix B. For illustration, in Figure 17 the time series for Area D are shown, where higher flow velocities occurred. At this location, flow velocities reached values up to 0.92 m/s, making Area D the most energetic one.

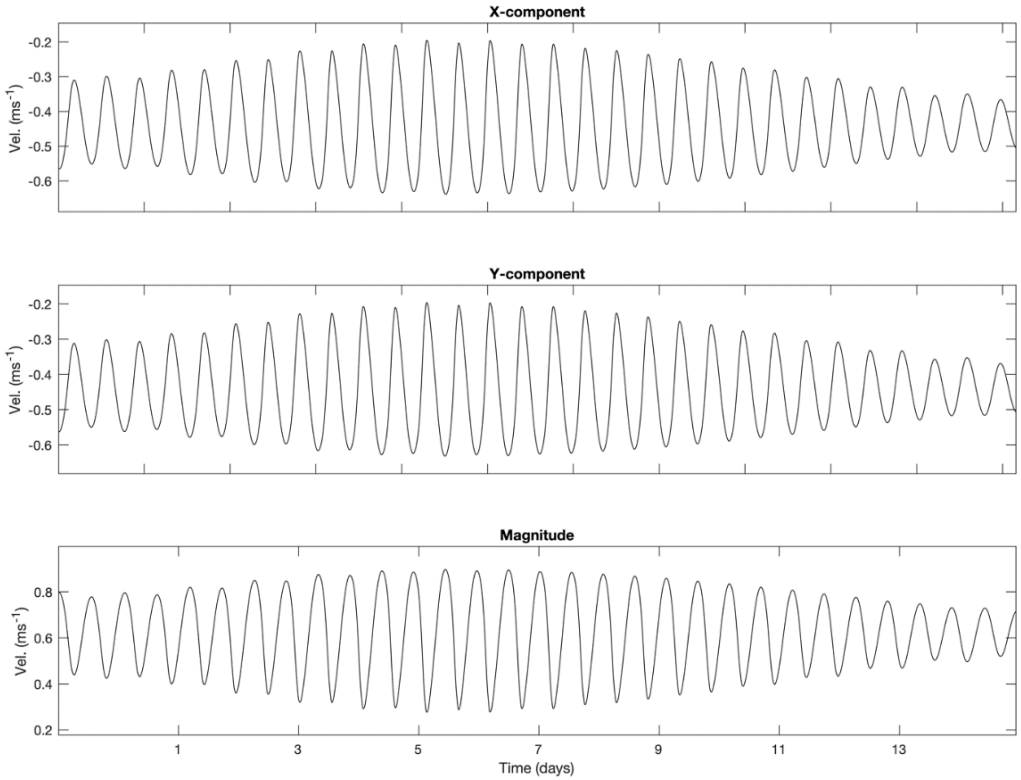

Figure 17. Components and magnitude of flow velocity at Area D (maximum TSE location).

As also confirmed by Figure 18—where the power density for all locations is provided—the results confirm that Area D is the most convenient location for the exploitation of the tidal and hydrokinetic resource. Additionally, it highlights the effects of cubic dependence of the power density with the tidal flow, since variations of 0.2 m/s in peak flow velocities translated into differences of almost 200 Wm^2 of available power density. As indicated in Figure 18, the mean power density for Area D was ca. 66 Wm^{-2} higher than in Areas A and B and ca. 39 Wm^{-2} higher than in Area C.

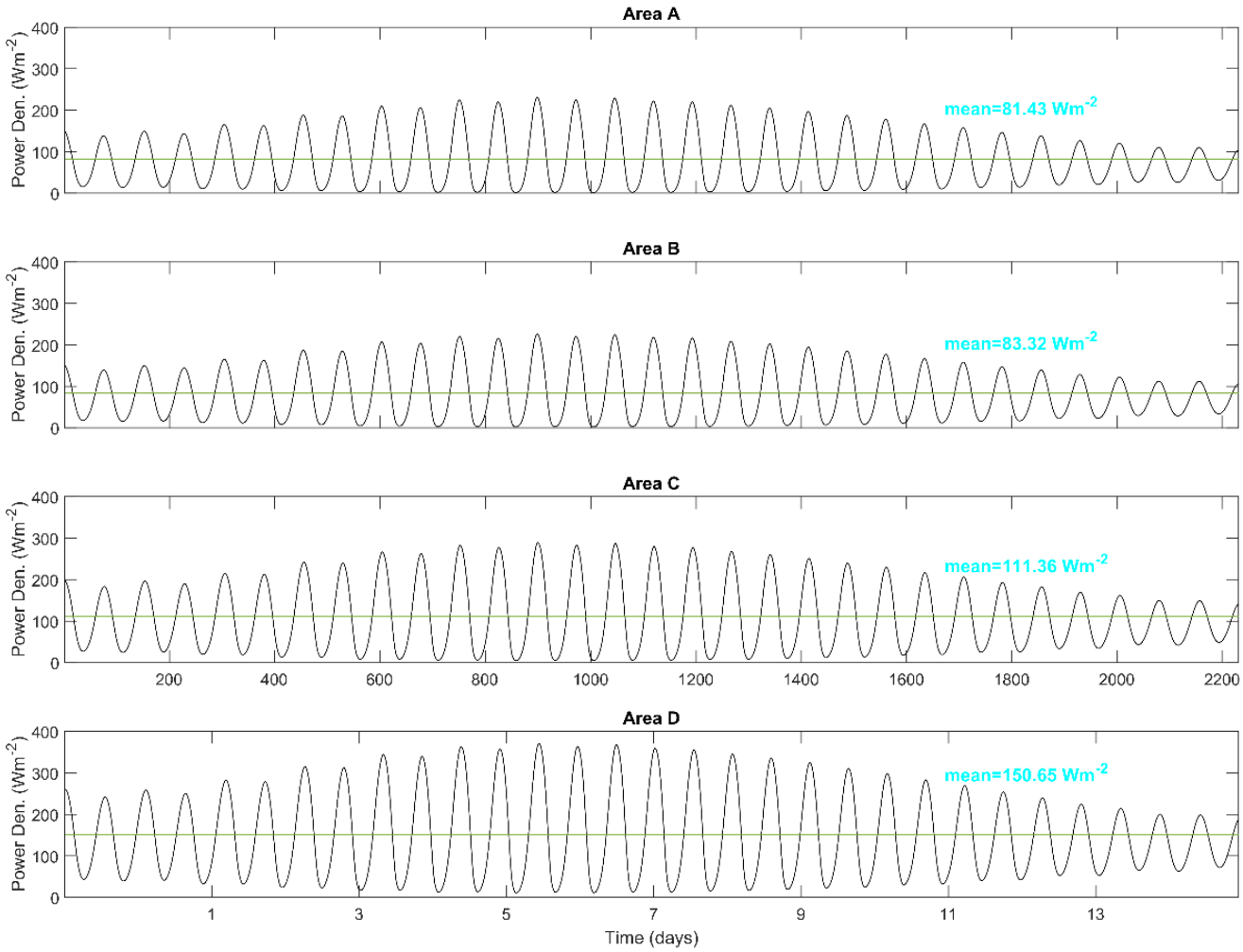

Figure 18. Power density time-series (spring-neap tidal cycle) for the areas of study.

4. Conclusions

A method for assessing the hydrokinetic resource potential of combined estuarine and river areas was defined and later applied to the specific Douro waterway case study for demonstration.

Following the proposed method, a high-resolution characterization of the tidal and river in-stream energy in the Douro, extending from Crestuma-Lever dam to Foz do Douro, was carried out. For this purpose, different scenarios were simulated by implementing a shallow-water numerical model, which was validated against field data available at several locations. Once the model was validated, the general description of the magnitude and distribution of the resource was depicted, and the influence of the river discharges on the total available energy was determined. It is shown that, for the case study region, the river runoffs are the main forcing factor and are responsible for a significant part of the total hydrokinetic energy resource. In addition, the intra-annual variations in the total available resource resulting from the variations of the river discharge throughout the year are quite significant.

The largest current magnitudes are found in the inner estuary, Area D (X = −38,200 m, Y = 163,600 m, PT-TM06/ETRS89), with maximum velocities during the ebb tide of ca. 1 m/s. In addition, other areas in the inner estuary with values exceeding 0.8 m/s exist. To have an accurate estimation of the total resource available, the power density was computed by simulating a complete year considering the intra-annual variations of the river discharges. The areas with the largest values of the power density roughly correspond

to the locations with peak flow velocities, with maximum figures of mean power density attained in the surroundings of Area D ca. 0.4 kW/m^2.

The selection of the best areas of interest for hydrokinetic energy exploitation was conducted based on an adaptation of the TSE index to the characteristics of the estuary and river under study. Again, the highest values of TSE $\approx$ 2.8 were found at Area D, with considerable variations amongst the remaining areas. However, the spatial variation of the TSE index leads to a better understanding of the distribution and availability of the hydrokinetic energy resource and based on it, the selection of specific areas could be conducted. More specifically, the areas with TSE index figures above specific thresholds were delimited and characterised.

In total, four areas (A, B, C and D) were identified and analysed to determine their suitability for hydrokinetic energy exploitation (high-resolution analysis). This analysis was conducted at specific locations corresponding to those providing the mean and maximum values of velocities and TSE within each specific area, over a complete mean spring-neap tidal cycle and considering mean river discharges. It is observed that the characteristics of the resource do not differ largely amongst all areas identified, except for Area D. It was found that areas A, B, and C, have a reduced tidal and hydrokinetic resource since flow velocities are limited. On the other hand, Area D presents a larger resource.

Nevertheless, a successive research phase must be carried out to confirm the technical and economic viability for the exploitation of all identified areas. Such a phase will comprehend a detailed analysis where further local restrictions, such as one represented by the navigational channel initially considered, should be furthermore analysed (e.g., constraints due to mooring points or berths). In addition, future work should focus on the selection or development of appropriate hydrokinetic in-stream technology for ensuring economically viable and sustainable projects. Technologies and future plants should be investigated, also taking into account potential environmental impacts, such as the ones on ecosystems and estuarine life. Solutions for mitigating all environmental impacts must be investigated and identified.

Overall, the method proposed showed to be effective for characterizing the hydrokinetic resource of the case study region and for selecting the most suitable places for hydrokinetic power generation. The approach was tailored for the mentioned case study region, and it may be almost directly applied to similar geographical areas. However, for another area of study presenting substantial diverse characteristics, it may be necessary to adapt or extend the proposed method so that specific additional major factors are taken into consideration. Despite this, further work should be oriented towards investigating methods for selecting the most suitable hydrokinetic in-stream technologies and for accurately assessing the economic viability of the possible development of small to medium-size hydrokinetic plants.

Author Contributions: Conceptualization, G.G., V.R. and P.R.-S.; methodology, G.G., V.R. and P.R.-S.; formal analysis, V.R. and G.G.; investigation, V.R., G.G., T.C.-C. and P.R.-S.; resources, V.R., T.C.-C. and G.G.; data curation, G.G., V.R. and T.C.-C.; writing—original draft preparation, G.G., V.R. and T.C.-C.; writing—review and editing, P.R.-S., V.R. and F.T.-P.; visualization, G.G., V.R. and T.C.-C.; supervision, P.R.-S.; project administration, P.R.-S. and F.T.-P.; funding acquisition, V.R., P.R.-S. and F.T.-P. All authors have read and agreed to the published version of the manuscript.

Funding: This research was funded by the project PORTOS (Ports Towards Energy Self-Sufficiency) (EAPA 784/2018) and co-financed by the Interreg Atlantic Area Program through the European Regional Development Fund. Furthermore, for this work, V.R. has been supported by the program of Stimulus of Scientific Employment Individual Support (CEECIND/03665/2018) from FCT (Portuguese national funds–Fundação para a Ciência e a Tecnologia).

Institutional Review Board Statement: Not applicable.

Informed Consent Statement: Not applicable.

Conflicts of Interest: The authors declare no conflict of interest.

Appendix A

Table A1 provides details of the tidal harmonics used in the study (A0, M2, S2, N2, K2, K1, O1, P1, Q1, MF, MM, M4, MS4, MN4) obtained from the TPXO 7.2 database.

Table A1. Major harmonic constituents at the open boundaries of the model.

	North Boundary		West Boundary		South Boundary	
	Amplitude (m)	**Phase (°)**	**Amplitude (m)**	**Phase (°)**	**Amplitude (m)**	**Phase (°)**
A0	1.800		1.800		1.800	
M2	1.067	73.48	1.066	73.51	1.065	73.08
S2	0.372	103.3	0.371	103.2	0.372	102.8
N2	0.225	55.40	0.225	55.40	0.225	55.10
K2	0.099	99.70	0.099	99.64	0.099	99.20
K1	0.073	64.76	0.073	64.71	0.073	64.26
O1	0.059	319.9	0.059	319.9	0.059	319.7
P1	0.021	56.05	0.021	56.02	0.021	55.74
Q1	0.019	265.4	0.019	265.3	0.019	265.1
MF	0.004	183.2	0.004	183.3	0.004	183.2
MM	0.002	189.8	0.003	189.8	0.002	189.8
M4	0.007	217.2	0.007	216.8	0.007	215.4
MS4	0.003	322.9	0.003	321.9	0.003	319.8
MN4	0.001	122.8	0.002	123.3	0.001	123.0

Appendix B

The results for the specific Area A are provided in Figure A1. Flow velocities range from 0.2 to 0.78 m/s, during a complete spring-neap tidal cycle.

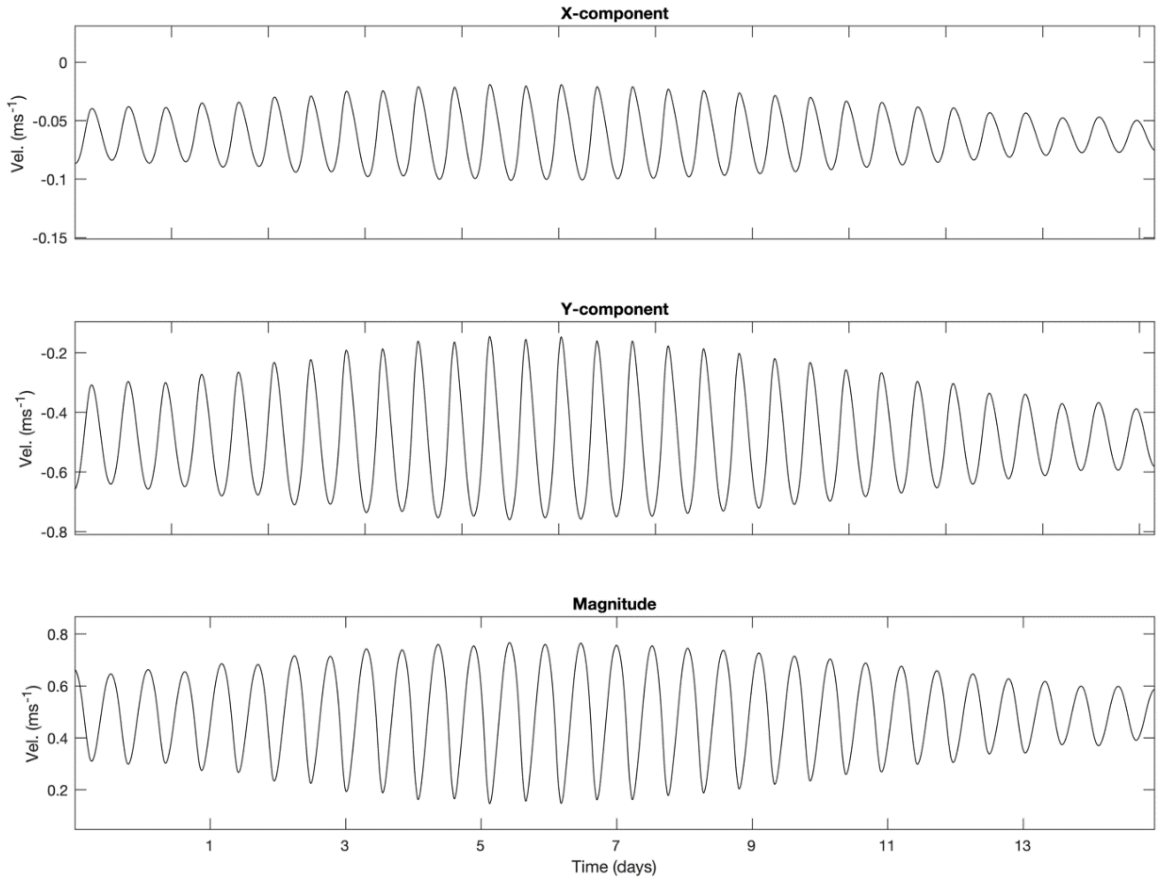

Figure A1. Components and magnitude of flow velocity at Area A (maximum TSE location).

Similarly, Figure A2 shows the flow velocity for a specific location of Area B, where the TSE reaches it maximum value. In this case, tidal velocities ranged from 0.2 to 0.76 m/s during the period of study.

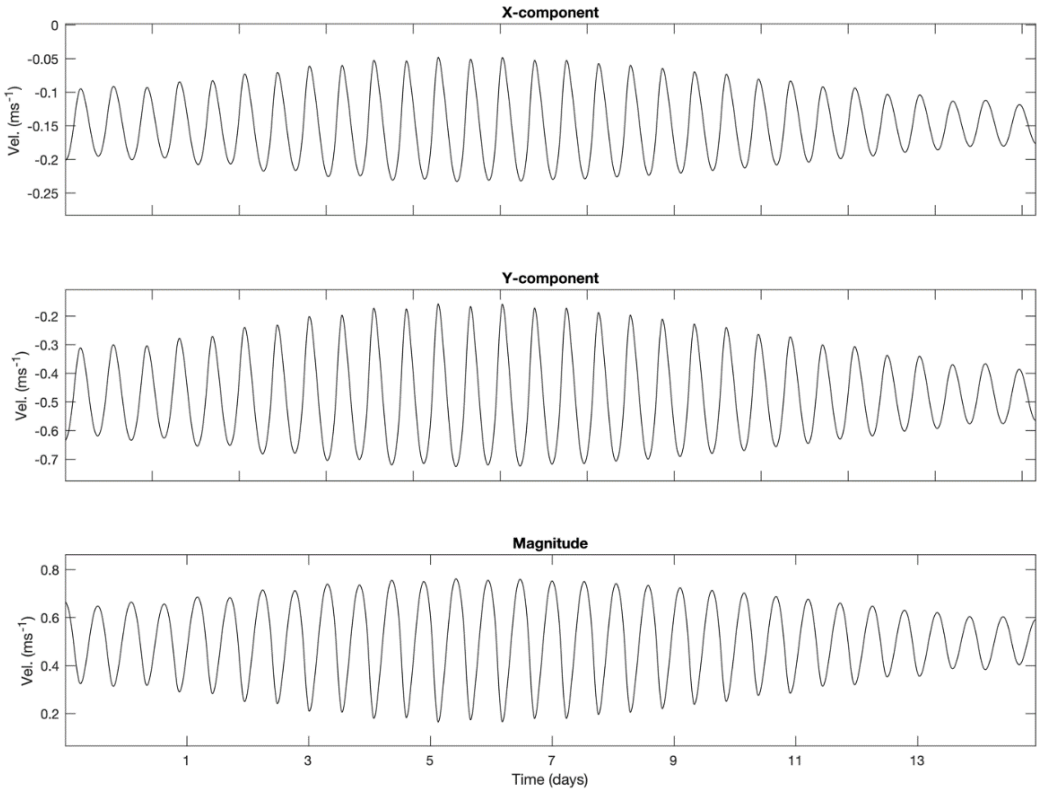

Figure A2. Components and magnitude of flow velocity at Area B (maximum TSE location).

The results obtained for Area C are shown in Figure A3. In this case, tidal velocities ranged from 0.2 to 0.83 m/s during the period of study.

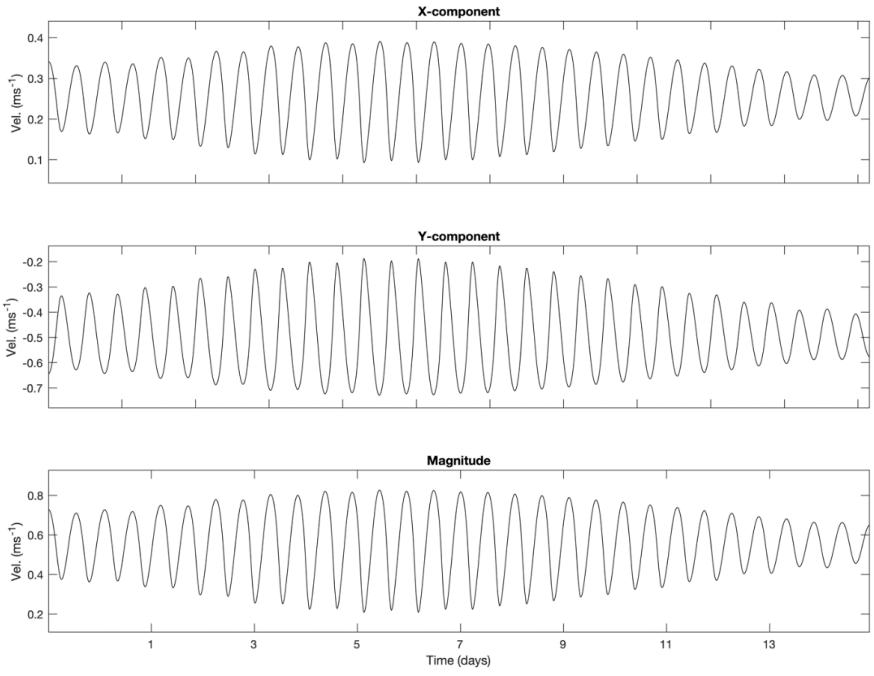

Figure A3. Components and magnitude of flow velocity at Area C (maximum TSE location).

References

1. Giannini, G. Modelling and Feasibility Study on Using Tidal Power with an Energy Storage Utility for Residential Needs. *Inventions* **2019**, *4*, 11. [CrossRef]
2. Burić, M.; Grgurić, S.; Mikulčić, H.; Wang, X. A numerical investigation of tidal current energy resource potential in a sea strait. *Energy* **2021**, *234*, 121241. [CrossRef]
3. Campbell, R.; Martinez, A.; Letetrel, C.; Rio, A. Methodology for estimating the French tidal current energy resource. *Int. J. Mar. Energy* **2017**, *19*, 256–271. [CrossRef]
4. Ramos, V.; Giannini, G.; Calheiros-Cabral, T.; Rosa-Santos, P.; Taveira-Pinto, F. Legal framework of marine renewable energy: A review for the Atlantic region of Europe. *Renew. Sustain. Energy Rev.* **2021**, *137*, 110608. [CrossRef]
5. Iyer, A.S.; Couch, S.J.; Harrison, G.P.; Wallace, A.R. Variability and phasing of tidal current energy around the United Kingdom. *Renew. Energy* **2013**, *51*, 343–357. [CrossRef]
6. Calero Quesada, M.C.; García Lafuente, J.; Sánchez Garrido, J.C.; Sammartino, S.; Delgado, J. Energy of marine currents in the Strait of Gibraltar and its potential as a renewable energy resource. *Renew. Sustain. Energy Rev.* **2014**, *34*, 98–109. [CrossRef]
7. Coiro, D.P.; Troise, G.; Ciuffardi, T.; Sannino, G. Tidal current energy resource assessment: The Strait of Messina test case. In Proceedings of the 2013 International Conference on Clean Electrical Power (ICCEP), Alghero, Italy, 11–13 June 2013.
8. Balestrino, F.; Coiro, D.P.; Giannini, G.; Giudice, D.; Troise, G. Resource assessment for the GEMSTAR tidal current energy harvester deployment in the strait of Messina. In Proceedings of the 13th European Wave and Tidal Energy Conference, Naples, Italy, 1–6 September 2019.
9. AQUARET European Resource Map. Available online: https://aquaret.com/indexcd1b.html?option=com_content&view=article&id=112&Itemid=255&lang=en (accessed on 27 October 2021).
10. Robins, P.E.; Neill, S.P.; Lewis, M.J.; Ward, S.L. Characterising the spatial and temporal variability of the tidal-stream energy resource over the northwest European shelf seas. *Appl. Energy* **2015**, *147*, 510–522. [CrossRef]
11. IEC. *Marine Energy Wave, Tidal and Other Water Current Converters-Part 2: Design Requirements for Marine Energy Systems*, 2nd ed.; International Electrotechnical Commission: Geneva, Switzerland, 2019.
12. Ramos, V.; Ringwood, J.V. Implementation and evaluation of the International Electrotechnical Commission specification for tidal stream energy resource assessment: A case study. *Energy Convers. Manag.* **2016**, *127*, 66–79. [CrossRef]
13. Vazquez, A.; Iglesias, G. A holistic method for selecting tidal stream energy hotspots under technical, economic and functional constraints. *Energy Convers. Manag.* **2016**, *117*, 420–430. [CrossRef]
14. Iglesias, G.; Sánchez, M.; Carballo, R.; Fernández, H. The TSE index—A new tool for selecting tidal stream sites in depth-limited regions. *Renew. Energy* **2012**, *48*, 350–357. [CrossRef]
15. Álvarez, M.; Ramos, V.; Carballo, R.; Arean, N.; Torres, M.; Iglesias, G. The influence of dredging for locating a tidal stream energy farm. *Renew. Energy* **2020**, *146*, 242–253. [CrossRef]
16. Ramos, V.; Carballo, R.; Sanchez, M.; Veigas, M.; Iglesias, G. Tidal stream energy impacts on estuarine circulation. *Energy Convers. Manag.* **2014**, *80*, 137–149. [CrossRef]
17. Janssen, R.; Arciniegas, G.; Alexander, K.A. Decision support tools for collaborative marine spatial planning: Identifying potential sites for tidal energy devices around the Mull of Kintyre, Scotland. *J. Environ. Plan. Manag.* **2015**, *58*, 719–737. [CrossRef]
18. Blunden, L.S.; Bahaj, A.S. Initial evaluation of tidal stream energy resources at Portland Bill, UK. *Renew. Energy* **2006**, *31*, 121–132. [CrossRef]
19. Pugh, D.T. *Tides, Surges and Mean Sea-Level (Reprinted with Corrections)*; John Wiley & Sons, Ltd.: Hoboken, NJ, USA, 1996; p. 486.
20. Ramos, V.; Iglesias, G. Performance assessment of Tidal Stream Turbines: A parametric approach. *Energy Convers. Manag.* **2013**, *69*, 49–57. [CrossRef]
21. Fouz, D.M.; Carballo, R.; Ramos, V.; Iglesias, G. Hydrokinetic energy exploitation under combined river and tidal flow. *Renew. Energy* **2019**, *143*, 558–568. [CrossRef]
22. Iglesias, I.; Venâncio, S.; Pinho, J.L.; Avilez-Valente, P.; Vieira, J.M.P. Two Models Solutions for the Douro Estuary: Flood Risk Assessment and Breakwater Effects. *Estuaries Coasts* **2019**, *42*, 348–364. [CrossRef]
23. Iglesias, I.; Bio, A.; Bastos, L.; Avilez-Valente, P. Estuarine hydrodynamic patterns and hydrokinetic energy production: The Douro estuary case study. *Energy* **2021**, *222*, 119972. [CrossRef]
24. Carballo, R.; Iglesias, G.; Castro, A. Numerical model evaluation of tidal stream energy resources in the Ría de Muros (NW Spain). *Renew. Energy* **2009**, *34*, 1517–1524. [CrossRef]
25. Deltares. *Deltares User Manual Delft3D-FLOW*; Deltares Ed.: Delft, The Netherlands, 2010.
26. Arakawa, A. Computational design for long-term numerical integration of the equations of fluid motion: Two-dimensional incompressible flow. *Part I. J. Comput. Phys.* **1966**, *1*, 119–143. [CrossRef]
27. Stelling, G.; Leendertse, J.J. Approximation of convective processes by cyclic ADI methods. In Proceedings of the Estuarine and Coastal Modeling, Tampa, FL, USA, 13–15 November 1992.
28. Wesseling, P. *Principles of Computational Fluid Dynamics*; Springer: Berlin/Heidelberg, Germany, 2001.
29. Egbert, G.; Bennett, A.; Foreman, M. TOPEX/Poseidon tides estimated using a global inverse model. *J. Geophys. Res.* **1995**, *99*, 24821–24852. [CrossRef]
30. Le Provost, C.; Bennett, A.F.; Cartwright, D.E. Ocean Tides for and from TOPEX/POSEIDON. *Science* **1995**, *267*, 639. [CrossRef]

31. Decastro, M.; Gómez-Gesteira, M.; Lorenzo, N.; Alvarez, I.; Crespo, A. Influence of atmospheric modes on coastal upwelling along the western coast of the Iberian Peninsula, 1985 to 2005. *Clim. Res.* **2008**, *36*, 169–179. [CrossRef]
32. Azevedo, I.C.; Duarte, P.M.; Bordalo, A.A. Pelagic metabolism of the Douro estuary (Portugal)—Factors controlling primary production. *Estuar. Coast. Shelf Sci.* **2006**, *69*, 133–146. [CrossRef]
33. Iglesias, G.; Carballo, R. Can the Seasonality of a Small River Affect a Large Tide-Dominated Estuary? The Case of Ría de Viveiro, Spain. *J. Coast. Res.* **2011**, *27*, 1170–1182. [CrossRef]
34. Souto, C.; Gilcoto, M.; Fariña-Busto, L.; Pérez, F.F. Modeling the residual circulation of a coastal embayment affected by wind-driven upwelling: Circulation of the Ría de Vigo (NW Spain). *J. Geophys. Res. Ocean.* **2003**, 108. [CrossRef]
35. Torres López, S.; Varela, R.A.; Delhez, E. Residual circulation and thermohaline distribution of the Ría de Vigo: A 3-D hydrodynamical model. *Sci. Mar.* **2001**, *65*, 277–289. [CrossRef]
36. Dias, J.M.; Lopes, J.F. Implementation and assessment of hydrodynamic, salt and heat transport models: The case of Ria de Aveiro Lagoon (Portugal). *Environ. Model. Softw.* **2006**, *21*, 1–15. [CrossRef]
37. Smith, S.D. Wind Stress and Heat Flux over the Ocean in Gale Force Winds. *J. Phys. Oceanogr.* **1980**, *10*, 709–726. [CrossRef]
38. Yelland, M.; Moat, B.; Taylor, P.K.; Pascal, R.; Hutchings, J.; Cornell, V.C. Wind Stress Measurements from the Open Ocean Corrected for Airflow Distortion by the Ship. *J. Phys. Oceanogr.* **1998**, *28*, 1511–1526. [CrossRef]
39. IH Website Instituto Hidrográfico. Available online: https://www.hidrografico.pt/ (accessed on 10 November 2021).
40. Fertahi, S.; Bouhal, T.; Rajad, O.; Kousksou, T.; Arid, A.; El Rhafiki, T.; Jamil, A.; Benbassou, A. CFD performance enhancement of a low cut-in speed current Vertical Tidal Turbine through the nested hybridization of Savonius and Darrieus. *Energy Convers. Manag.* **2018**, *169*, 266–278. [CrossRef]